

See discussions, stats, and author profiles for this publication at: <https://www.researchgate.net/publication/259950858>

Evidence for deposition of 10 million tonnes of impact spherules across four continents 12,800 y ago

Article · January 2013

DOI: 10.1073/pnas.1301760110/-/DCSupplemental

CITATIONS

22

READS

751

10 authors, including:



James H. Wittke

Northern Arizona University

118 PUBLICATIONS 2,221 CITATIONS

[SEE PROFILE](#)



James Weaver

Harvard University

262 PUBLICATIONS 20,110 CITATIONS

[SEE PROFILE](#)



Ted E. Bunch

Retired

266 PUBLICATIONS 6,406 CITATIONS

[SEE PROFILE](#)



James P Kennett

University of California, Santa Barbara

1,715 PUBLICATIONS 27,713 CITATIONS

[SEE PROFILE](#)

Some of the authors of this publication are also working on these related projects:



Younger Dryas Impact Hypothesis [View project](#)



Paleocoastal Occupations of California's Channel Islands [View project](#)

Evidence for deposition of 10 million tonnes of impact spherules across four continents 12,800 y ago

James H. Wittke^a, James C. Weaver^b, Ted E. Bunch^{a,1}, James P. Kennett^c, Douglas J. Kennett^d, Andrew M. T. Moore^e, Gordon C. Hillman^f, Kenneth B. Tankersley^g, Albert C. Goodyear^h, Christopher R. Mooreⁱ, I. Randolph Daniel, Jr.^j, Jack H. Ray^k, Neal H. Lopinot^k, David Ferraro^l, Isabel Israde-Alcántara^m, James L. Bischoffⁿ, Paul S. DeCarli^o, Robert E. Hermes^{p,2}, Johan B. Kloosterman^{q,2}, Zsolt Revay^r, George A. Howard^s, David R. Kimbel^t, Gunther Kletetschka^u, Ladislav Nabelek^{u,v}, Carl P. Lipo^w, Sachiko Sakai^w, Allen West^x, and Richard B. Firestone^y

^aGeology Program, School of Earth Science and Environmental Sustainability, Northern Arizona University, Flagstaff, AZ 86011; ^bWysys Institute for Biologically Inspired Engineering, Harvard University, Cambridge, MA 02138; ^cDepartment of Earth Science and Marine Science Institute, University of California, Santa Barbara, CA 93106; ^dDepartment of Anthropology, Pennsylvania State University, University Park, PA 16802; ^eCollege of Liberal Arts, Rochester Institute of Technology, Rochester, NY 14623; ^fInstitute of Archaeology, University College London, London WC1H0PY, United Kingdom; ^gDepartments of Anthropology and Geology, University of Cincinnati, Cincinnati, OH 45221; ^hSouth Carolina Institute of Archaeology and Anthropology, University of South Carolina, Columbia, SC 29208; ⁱSavannah River Archaeological Research Program, South Carolina Institute of Archaeology and Anthropology, University of South Carolina, New Ellenton, SC 29809; ^jDepartment of Anthropology, East Carolina University, Greenville, NC 27858; ^kCenter for Archaeological Research, Missouri State University, Springfield, MO 65897; ^lViejo California Associates, Joshua Tree, CA 92252; ^mDepartamento de Geología y Mineralogía, Edificio U4, Instituto de Investigaciones Metalúrgicas, Universidad Michoacana de San Nicolás de Hidalgo, C. P. 58060, Morelia, Michoacán, México; ⁿUS Geological Survey, Menlo Park, CA 94025; ^oSRI International, Menlo Park, CA 94025; ^pLos Alamos National Laboratory, Los Alamos, NM 87545; ^qExploration Geologist, 1016 NN, Amsterdam, The Netherlands; ^rForschungszentrum für Neutronenphysik und Neutronenphysik, Technische Universität München, 85748 Garching, Germany; ^sRestoration Systems, LLC, Raleigh, NC 27604; ^tKimstar Research, Fayetteville, NC 28312; ^uFaculty of Science, Charles University in Prague, 12843 Prague, Czech Republic; ^vInstitute of Geology, Academy of Sciences of the Czech Republic, Public Research Institute, 16500 Prague, Czech Republic; ^wInstitute for Integrated Research in Materials, Environments, and Society, California State University, Long Beach, CA 90840; ^xGeoScience Consulting, Dewey, AZ 86327; and ^yLawrence Berkeley National Laboratory, Berkeley, CA 94720

Edited* by Steven M. Stanley, University of Hawaii, Honolulu, HI, and approved April 9, 2013 (received for review January 28, 2013)

Airbursts/impacts by a fragmented comet or asteroid have been proposed at the Younger Dryas onset (12.80 ± 0.15 ka) based on identification of an assemblage of impact-related proxies, including microspherules, nanodiamonds, and iridium. Distributed across four continents at the Younger Dryas boundary (YDB), spherule peaks have been independently confirmed in eight studies, but unconfirmed in two others, resulting in continued dispute about their occurrence, distribution, and origin. To further address this dispute and better identify YDB spherules, we present results from one of the largest spherule investigations ever undertaken regarding spherule geochemistry, morphologies, origins, and processes of formation. We investigated 18 sites across North America, Europe, and the Middle East, performing nearly 700 analyses on spherules using energy dispersive X-ray spectroscopy for geochemical analyses and scanning electron microscopy for surface microstructural characterization. Twelve locations rank among the world's premier end-Pleistocene archaeological sites, where the YDB marks a hiatus in human occupation or major changes in site use. Our results are consistent with melting of sediments to temperatures >2,200 °C by the thermal radiation and air shocks produced by passage of an extraterrestrial object through the atmosphere; they are inconsistent with volcanic, cosmic, anthropogenic, lightning, or authigenic sources. We also produced spherules from wood in the laboratory at >1,730 °C, indicating that impact-related incineration of biomass may have contributed to spherule production. At 12.8 ka, an estimated 10 million tonnes of spherules were distributed across ~50 million square kilometers, similar to well-known impact strewnfields and consistent with a major cosmic impact event.

Clovis-Folsom | lechatelierite | tektite | wildfires

An increasing body of evidence suggests that major cosmic airbursts/impacts with Earth occurred at the onset of the Younger Dryas (YD) episode, triggering abrupt cooling and causing major environmental perturbations that contributed to megafaunal extinctions and human cultural changes. (Note that “airburst/impact” is used to refer to a collision by a cosmic body with Earth’s atmosphere, producing an extremely high-energy aerial disintegration that may be accompanied by numerous small crater-forming impacts by the fragments.) The impact hypothesis

originated from observations of peaks in Fe-rich and Al-Si-rich impact spherules, nanodiamonds, and other unusual impact tracers discovered in the Younger Dryas boundary layer (YDB), a sedimentary stratum typically only a few centimeters thick. The hypothesis was first proposed by Firestone et al. (1) and expanded upon by Kennett et al. (2–4), Kurbatov et al. (5), Anderson et al. (6), Israde et al. (7), Bunch et al. (8), and Jones and Kennett (9). Formerly, the date of the impact event was reported as 10.9 ± 0.145 ka (radiocarbon), calibrated as 12.9 ± 0.10 ka B.P., using the then-standard calibration curve IntCal04. (Unless otherwise noted, all dates are presented as calibrated or calendar

Significance

We present detailed geochemical and morphological analyses of nearly 700 spherules from 18 sites in support of a major cosmic impact at the onset of the Younger Dryas episode (12.8 ka). The impact distributed ~10 million tonnes of melted spherules over 50 million square kilometers on four continents. Origins of the spherules by volcanism, anthropogenesis, authigenesis, lightning, and meteoritic ablation are rejected on geochemical and morphological grounds. The spherules closely resemble known impact materials derived from surficial sediments melted at temperatures >2,200 °C. The spherules correlate with abundances of associated melt-glass, nanodiamonds, carbon spherules, aciniform carbon, charcoal, and iridium.

Author contributions: J.H.W., J.C.W., T.E.B., J.P.K., D.J.K., A.M.T.M., G.C.H., K.B.T., A.C.G., D.F., I.I.-A., R.E.H., J.B.K., Z.R., D.R.K., G.K., C.P.L., S.S., A.W., and R.B.F. designed research; J.H.W., J.C.W., T.E.B., J.P.K., D.J.K., A.M.T.M., G.C.H., K.B.T., A.C.G., C.R.M., I.R.D., J.H.R., N.H.L., D.F., I.I.-A., J.L.B., P.S.D., R.E.H., J.B.K., Z.R., G.A.H., D.R.K., G.K., L.N., C.P.L., S.S., A.W., and R.B.F. performed research; J.H.W., J.C.W., T.E.B., J.P.K., D.J.K., A.M.T.M., K.B.T., A.C.G., D.F., I.I.-A., P.S.D., R.E.H., J.B.K., Z.R., G.K., L.N., C.P.L., S.S., A.W., and R.B.F. analyzed data; and J.H.W., J.C.W., T.E.B., J.P.K., D.J.K., A.M.T.M., K.B.T., A.C.G., C.R.M., I.R.D., J.H.R., N.H.L., D.F., I.I.-A., J.L.B., P.S.D., R.E.H., J.B.K., G.A.H., D.R.K., G.K., A.W., and R.B.F. wrote the paper.

The authors declare no conflict of interest.

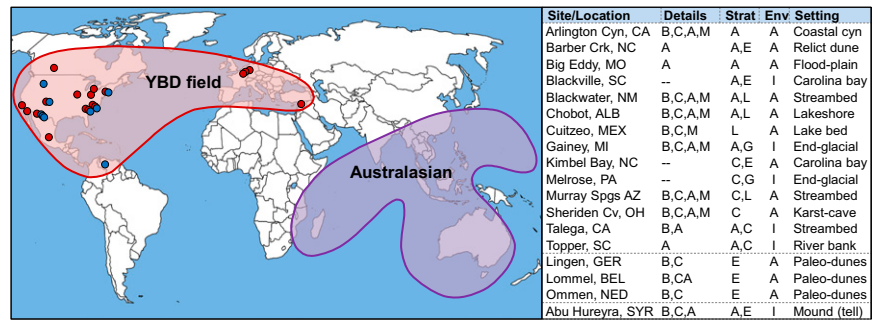
*This Direct Submission article had a prearranged editor.

¹To whom correspondence should be addressed. E-mail: tbea1@cableone.net.

²Retired.

This article contains supporting information online at www.pnas.org/lookup/suppl/doi:10.1073/pnas.1301760110/-DCSupplemental.

Fig. 1. YDB impact field, based on data from 27 locations. In the YDB strewnfield (red), there are 18 YDB sites in this study (red dots; see table on *Right*). Eight independent studies have found spherules and/or scoria-like objects at nine additional sites (blue dots) located in Arizona, Montana, New Mexico, Maryland, South Carolina, Pennsylvania, Mexico, and Venezuela. The largest accepted impact strewnfield, the Australasian (purple), is shown for comparison with each strewnfield covering ~50 million square kilometers or ~10% of the planet. Table shows location of sites and lists site details (A, archeological material; B, black mat; C, charcoal; M, megafaunal remains, present either at the sampling location or in the vicinity). Also given are stratigraphic settings (Strat: A, alluvial; C, colluvial; E, eolian; G, glacial; and L, lacustrine) and relative physical stability of depositional paleoenvironments (Env: A, active, e.g., riverine, lacustrine, or eolian; I, inactive).



kiloannum.) Using the most recent curve, IntCal09, the same radiocarbon date calibrates as 12.8 ± 0.15 ka.

Impact-related spherules have long been considered one of the most distinctive proxies in support of this hypothesis. However, despite increasing evidence for YDB peaks in impact spherules, their presence and origin remain disputed (10, 11). In the latest example of this dispute, Boslough et al. (ref. 12, p. 21) stated that “magnetic microspherule abundance results published by the impact proponents have not been reproducible by other workers.” However, the authors neglected to cite nine independent spherule studies on two continents (shown in Fig. 1) that reported finding significant YDB spherule abundances, as summarized in high-profile previously published papers by Israde et al. (7), Bunch et al. (8), and LeCompte et al. (13). The nine additional sites are located in Arizona (14–16), Montana[†], New Mexico, Maryland, South Carolina (13), Pennsylvania (17); Mexico[‡], and Venezuela (18–21). In response to such claims, we here present the results of one of the most comprehensive investigations of spherules ever undertaken to address questions of geochemical and morphological characteristics, distribution, origin, and processes involved in the formation of YDB spherules.

We refer here to all melted, rounded-to-subrounded YDB objects as spherules. At a few locations, spherules are found in association with particles of melted glass called scoria-like objects (SLOs), which are irregular in shape and composed of highly vesicular, siliceous melt-glass, as described in Bunch et al. (8). Collectively, YDB spherules and SLOs are here referred to as YDB objects. Peaks in spherules were observed at the onset of the YD at 27 sites—18 sites in this study and nine sites independently studied in North and South America (Fig. 1). Whereas most independent studies concluded that the YDB spherules formed during a high-temperature cosmic impact event, one study by Surovell et al. (10) was unable to find any YDB spherule peaks at seven sites. However, LeCompte et al. (13) repeated the analyses at three of those sites and verified the previous observations (1), concluding that the inability of Surovell et al. (10) to find YDB spherule peaks resulted from not adhering to the prescribed extraction protocol (1, 7). For example, Surovell et al. did not conduct any analyses using scanning electron microscopy (SEM) and energy dispersive X-ray spectroscopy (EDS), a necessary procedure clearly specified by Firestone et al. (1). In another study, Pigati et al. (14) confirmed the previously reported YDB peak in spherules at Murray

Springs, Arizona, and also claimed to find several non-YDB spherule peaks in Chile. However, the Chilean sites are known to contain abundant volcanic spherules (22), and yet Pigati et al. (14) did not perform any analyses of candidate spherules with SEM and EDS, which are crucial for differentiating impact-related YDB spherules from volcanic spherules, detrital magnetic grains, framboids, and other spherule-like particles.

In another study, Pinter et al. (11) claimed to have sampled the YDB layer at a location “identical or nearly identical” with the location reported by Kennett (2–4), as part of three studies that reported finding no YDB spherules or nanodiamonds (11, 23, 24). However, the published Universal Transverse Mercator coordinates reveal that their purported continuous sequence is actually four discontinuous sections. These locations range in distance from the site investigated by Kennett et al. (2) by 7,000 m, 1,600 m, 165 m, and 30 m (*SI Appendix, Fig. S1B*), clearly showing that they did not sample the YDB site of Kennett et al. (2). Furthermore, this sampling strategy raises questions about whether Pinter et al. (11) sampled the YDB at all, and may explain why they were unable to find peaks in YDB magnetic spherules, carbon spherules, or nanodiamonds.

It is widely accepted that spherules form during cosmic impacts (25–29), and spherules also form as ablation products from the influx of meteorites and cosmic dust. However, not all terrestrial spherules are cosmic in origin; abundant spherules commonly occur throughout the geological record due to non-impact processes. For example, spherules and glass can be produced by continental volcanism (30), hydrovolcanism (31), metamorphism (29), lightning strikes (18, 32), and coal seam fires (32). In addition, detrital magnetite and quartz grains are frequently rounded from wind and water action and may appear spherulitic, as can authigenic framboids, all of which are common in sediments (33). Spherules and melt-glasses can also be produced anthropogenically, especially by coal-fired power plants and smelters (34), although these are normally restricted to surface deposits of industrial age (<300 y old). Al-Si-rich spherules have been produced under laboratory conditions from the combustion of charcoal at ~1,600–2,000 °C (35). Also, numerous spherules and melt-glass have been produced in atomic explosions (36, 37), including the Trinity detonation in New Mexico in 1945, where the airburst produced spherules similar to those from the Tunguska cosmic airburst in 1908 (8, 38). More specifically, the Trinity explosion was a surface burst because the aerial fireball intersected the ground.

In summary, although there are many processes by which spherules can be produced, each type of spherule exhibits a unique set of geochemical, morphological, and/or microstructural characteristics that allow it to be differentiated from impact-related spherules. All types appear similar to YDB spherules under a light microscope, and so, the use of SEM/EDS is crucial for the differentiation of YDB impact spherules from other types.

[†]Baker DW, Miranda PJ, Gibbs KE, Montana evidence for extra-terrestrial impact event that caused Ice-Age mammal die-off, American Geophysical Union Spring Meeting, May 27–30, 2008, Ft. Lauderdale, FL, abstr P41A-05.

[‡]Scruggs MA, Raab LM, Murowchick JS, Stone MW, Niemi TM, Investigation of sediment containing evidence of the Younger Dryas Boundary (YDB) Impact Event, El Carrizal, Baja California Sur, Mexico, Geological Society of America Abstracts with Programs, vol 42, no. 2, p 101 (abstr).

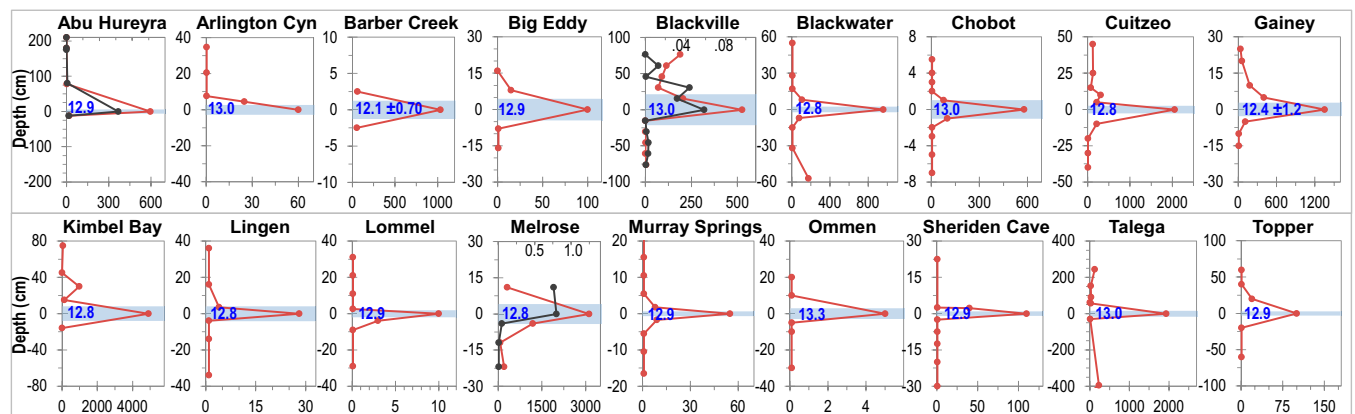


Fig. 2. Stratigraphic distribution. Abundances of spherules by site (red lines), plotted on lower x axis in number per kilogram relative to the YDB depth at 0 cm. SLO concentrations (black lines) are plotted on upper x axis in grams per kilogram (*SI Appendix, Table S3*). Thickness of sample containing YDB is indicated by blue bar. Dates for YDB layer are in blue, as determined by age-depth models (*SI Appendix, Table S1*).

Results and Discussion

Site Details. To quantitatively investigate YDB spherules, we examined 18 sites across three continents (Fig. 1), selecting most because they contained independently dated chronostratigraphic profiles that spanned the onset of the YD at ~ 12.8 ka, thus providing identifiable candidate strata for the YDB layer. Investigations of spherules were previously conducted at seven of those sites (1, 10, 11, 13). The stratigraphy, chronology, and archaeological significances of each site are summarized in Fig. 1. Also, each of 15 sites is described in detail in *SI Appendix, Figs. S1–S15*; the other three sites were previously described in Bunch et al. (8).

The YDB sequences were dated by accelerator-mass spectrometry radiocarbon dating at 11 of 18 sites, and optically stimulated luminescence (OSL) or thermal luminescence at six others. Eleven new radiometric and OSL dates for four sites are presented here, along with 67 previously published dates for the other sites (*SI Appendix, Table S1*); most sites are well dated, but several have large uncertainties. The stratigraphic position of the YDB for each site is determined from its interpolated age-depth model, and overall, the interpolated ages of the YDB layers are consistent with the revised age of ~ 12.8 ka.

Other criteria helped confirm the identification of the YDB layer, including the stratigraphic distribution of archaeological artifacts, found either at the sampling location or in the vicinity for 12 sites, including 10 in North America that contain projectile points and other artifacts from Paleoamerican cultures (Clovis, Folsom, Gainey, and Archaic projectile points are shown in *SI Appendix, Figs. S2–S5, S11, S13, and S15*); some are well-documented Clovis sites, displaying projectile points that establish a date range of 12.80–13.25 ka (39). Clovis points have never been found in situ in strata younger than ~ 12.8 ka. One site was radiometrically undated, but abundant, temporally diagnostic Clovis Paleoamerican artifacts indicated the likely stratigraphic position of the YDB at the top of the artifact layer, as later confirmed by a peak in impact spherules. Furthermore, identification of the YDB layer was aided by visual changes in lithology, including the presence at 12 sites of darker lithologic units, e.g., the “black mat” layer (40), along with charcoal abundance peaks at 11 sites.

Across North America, the YDB layer coincides with the extinction of late-Pleistocene megafauna, including mammoth (*Mammuthus*), American horse (*Equus*), American camel (*Camelops*), and dire wolf (*Canis dirus*), which have never been found in known chronostratigraphic context that is <12.8 ky old (40).

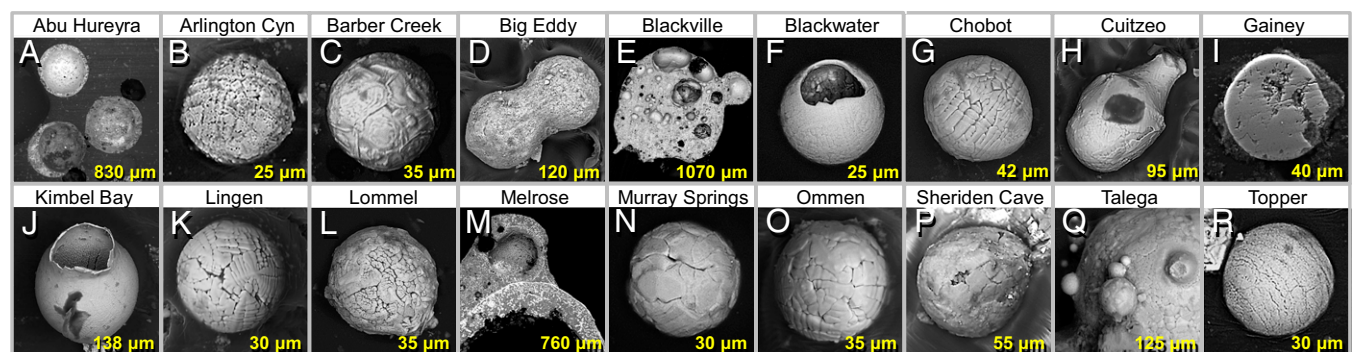


Fig. 3. YDB spherules from 18 sites. SEM images illustrate the wide variety of sizes, shapes, and microstructures of YDB spherules. Diameters are in yellow. EDS compositional percentages corresponding to the letter designations of these 36 YDB spherules are in *SI Appendix, Table S5*. Most spherules are rounded, but there are also dumbbells (*D*), bottle shapes (*H*), gourd shapes (*J*), and ovoids (*P*). Most small spherules are solid, although a few are hollow (*F* and *J*), whereas most large spherules are vesicular and/or hollow (*A*, *E*, and *M*). A large number of spherules were cross-sectioned ($n = 137$ EDS; *A*, *E*, *I*, and *M*); all others were analyzed whole ($n = 335$ EDS). Lechatelierite and flow marks (schlieren) that formed at $>2,200$ °C were observed in spherules from three sites (*A*, *E*, and *M*). Many large spherules display accretion with other spherules (*E*, *M*, and *Q*) and microcratering by smaller spherules (*Q*). Interior and exterior compositions of both spherules are similar, but occasionally, Fe-rich material (thin, light-colored bands) migrated or accreted to the outside of the spherule while molten (*M*). Some spherules have high percentages of TiO_2 (*B*, *L*, and *R*; averaging 42 wt%), inconsistent with anthropogenic and most cosmic origins, but consistent with impact melting of titanomagnetite or ilmenite.

Mega-faunal bones, found either at the sampling location or in the vicinity at five sites, were dated approximately to the YD onset (40) and are associated with temporally diagnostic projectile points. Abu Hureyra, the archaeological site in Syria, is unique in representing the origin of domesticated plant cultivation that began at ~12.8 ka, when inhabitants transitioned from hunting-gathering to hunting-cultivating. The western European locations in Germany, Belgium, and the Netherlands were coeval with the decline near 12.8 ka of the Magdalenian and related cultures, known for their elaborate cave paintings and intricate carvings (6).

Bulk sediment was processed in aliquots averaging 228 g (range: 10–1,600 g). On occasion, material was limited, e.g., due to use of small-diameter coring tools. For the 15 noncored sites, the YDB layer was contained in samples that averaged 3.9 cm in thickness (median: 5 cm; range: 1–8 cm). At one hand-cored site, the YDB layer was contained in a sample that was 15-cm thick, and the machine-cored sample was 30-cm thick. The burial depth of the YDB layer averaged 2.52 m (median 1.50 m; range: 0.13–15.00 m). Sampling details are in *SI Appendix, Table S2*.

Abundances and Compositions of Magnetic Grains. After analyzing the magnetic grains and the YD spherules they contain, Firestone et al. (1) and LeCompte et al. (13) reported strong to moderate correlation, respectively, between abundances of the two proxies. To test that correlation, we created slurries of bulk sediment and magnetically extracted the magnetic grain fraction. The maximum YDB magnetic grain concentration in bulk sediments ranged from 0.4 to 73.6 g/kg (average: 7.2 g/kg), and in most samples, concentrations decreased outside the YDB to 0.02–8.9 g/kg (average: 2.0 g; *SI Appendix, Table S3*). Some magnetic grains (but not spherules) were analyzed using neutron activation analysis and prompt gamma activation analysis (*SI Appendix, Table S4*), indicating they are dominantly comprised of magnetite and titanomagnetite. For seven sites, a peak in magnetic grains coincided with a peak in magnetic spherules, whereas for seven other sites, they were found in immediately adjacent layers. For four sites, they were not adjacent. These results support a moderate correlation between peaks in spherules and magnetic grains, indicating that the YDB layer is enriched in both.

Abundances and Stratigraphic Distribution of Spherules. We investigated abundances of YDB spherules at 18 sites, seven of which were common to Firestone et al. (1) and two to LeCompte et al. (13). We identified and measured 771 YDB objects, of which 684 were spherules and 87 were SLOs. Spherule diameters ranged from 5 μm to 5.5 mm (average: 135 μm) with ~50% $\leq 30 \mu\text{m}$ (see distribution in *SI Appendix, Fig. S16*). YDB SLOs ranged from 300 μm to 11.75 mm, averaging 2.6 mm (8). Concentrations of spherules in the YDB layer varied widely from 5 to 4,900 spherules per kilogram (average: 955/kg; median: 388). At stratigraphic levels more distant above or below the YDB, spherules were absent or rare, indicating that the influx of normal cosmic spherules was negligible. Layers adjacent to the YDB typically contained lower concentrations of spherules, whose presence is most likely due to redeposition and/or bioturbation from the YDB layer. See Fig. 2 for graphs of spherule and SLO concentrations. At every site investigated, the abundance peak in spherules coincided with the YDB depths previously reported, although estimated concentrations varied from those reported by Firestone et al. (1) by an average of 56% (range: 10–160%), and from LeCompte et al. (13) by 94% (range 19–168%), presumably due to variable deposition, preservation, and preparation. All sites investigated exhibited abundance peaks in spherules at or close to ~12.8 ka, as interpolated in the age-depth models.

Morphologies of Magnetic Spherules. To investigate potential formation mechanisms of YDB spherules, we examined their morphologies using light microscopy followed by SEM. Three

types of spherulitic objects were typically encountered in the sedimentary profiles: (i) nonimpact, quasi-spherical, detrital magnetite grains that are typically black or dark gray and are common throughout sedimentary profiles; (ii) nonimpact, authigenic framboidal spherules that are typically black, gray, or rusty red in color and are common throughout sediments; and (iii) YDB spherules that are black, brown, red, blue, green, gray, tan, or white, ranging in clarity from opaque to transparent; these were confined to the YDB layer and closely adjacent strata. Light photomicrographs revealed that all three types are rounded and reflective (*SI Appendix, Fig. S17*). SEM imagery of the rounded detrital magnetite grains indicated that formerly euhedral monocrystals are now rounded but still display remnant faceting, thus eliminating them as impact products. Authigenic framboids appear round when viewed optically, but SEM imaging reveals distinctive blocky surface texturing that results from slow crystalline growth, thus eliminating them as impact spherules. Accurate differentiation of YDB spherules from magnetite grains and framboids is impossible by light microscopy alone and requires the use of SEM/EDS.

There are several accepted groups of melt-products ascribed to known impacts that are relevant to this study; the first is a condensation group, in which glassy impact spherules can condense from rocks that were vaporized during an impact. Such spherules can appear as multiples (i.e., are accretionary), are typically nonvesicular, and do not contain lechatelierite (27, 41). The second is a melt-and-quench group, in which compressive and frictional heating by the impactor subjected the target rocks and impactor to high temperatures that boiled both of them (41). The liquefied rock was then ejected and aerodynamically shaped into spherules, teardrops, ovoids, and dumbbells that are often vesicular and often contain lechatelierite. Collectively, these are called splash-form tektites or microtektites (8, 27, 41). Most YDB spherules are highly reflective spheroids similar to those in each group, but ~10–20% of them exhibit complex aerodynamic shapes, consistent only with splash-formed microtektites. The shapes and surface textures of all YDB spherules are similar to those formed in the Cretaceous–Paleogene extinction (KPg) impact ~65 Ma (28), Chesapeake Bay impact at ~35 Ma (27), Meteor Crater at ~50 ka (8), Tunguska airburst in 1908 (8), and Trinity atomic airburst (8). The similarity of YDB spherules to those from known airbursts (e.g., Tunguska and Trinity) suggests they were caused by an impact/airburst. See SEM images in Fig. 3 and *SI Appendix, Figs. S17, S18, S24, and S25*.

Nearly all of the largest YDB spherules (maximum: 5.5 mm) are vesicular, consistent with outgassing at high temperatures, followed by rapid cooling that preserved the gas bubbles, and in some samples formed quench crystals within the bubbles. The prevalence of vesicles decreases with spherule diameter, and most small spherules <50 μm in diameter are solid. All Fe-rich spherules and some Al-rich ones display dendritic crystals on their surfaces, consistent with high-temperature melting and quenching (8). Most Al–Si-rich spherules are smooth, but sometimes display flow marks, or schlieren, along with melted SiO₂ (lechatelierite) inclusions, both indicative of high-temperature melting at >2,200 °C (8). Approximately 10% of YDB spherules display evidence of accretion (nondestructive fusion of two or more spherules) and/or collisions (destructive interactions between two or more spherules) (8). Destructive collisions require high differential velocities between spherules, and therefore, they frequently result from impacts and meteoritic ablation, but not from other processes, such as volcanism and anthropogenesis (8). SEM images of spherules from four sites illustrate the results of both processes (8). Together, the collective shapes, surface textures, and inferred formation temperatures of YDB spherules are inconsistent with known volcanic or anthropogenic spherules but are consistent with impact spherules.

Geochemical and Petrological Evidence for Spherule Origin. We conducted 750 SEM/EDS analyses (472 on YDB spherules, 153 on SLOs, and 125 on reference materials, including fly ash). Spherules that were ≥ 50 μm in diameter were typically analyzed both whole and in cross-section ($n = 269$ EDS). Due to technical difficulties in making cross-sections of very small objects, spherules < 50 μm in diameter were only analyzed whole ($n = 203$ EDS). This analysis is consistent with the methodology of Brownlee et al. (42), who did not obtain cross-sections for the subset of 500 cosmic spherules < 50 μm in diameter that were recovered from deep-sea sediments, polar ice, and the stratosphere.

SEM/EDS analyses of candidate spherules provided oxide weight percentages (wt%) for 13 elements. Spherule compositions ranged from homogeneous to heterogeneous, with the three most abundant oxides being iron oxide (expressed as total FeO) with an average of 44.9 wt% (range: 0–100%); silica (SiO_2) averaged 30.9 wt% (range: 0–95%); and aluminum oxide (Al_2O_3) averaged 12.2 wt% (range: 0–65%). The other 10 oxides ranged from 0.1 to 3.5 average wt% (SI Appendix, Table S6). The oxide concentrations were inferred from normal oxidation states and not measured directly, making it likely that other compounds are also present. EDS compositional percentages for 36 selected spherules, including those in Fig. 3, are in SI Appendix, Table S5. Variation diagrams comparing SiO_2 to FeO, CaO, and Al_2O_3 are shown in SI Appendix, Fig. S19. Many of the higher oxide concentrations were found in melted mineral inclusions, e.g., Al_2O_3 at 65 wt% appeared as mullite and sillimanite crystals; CaO at 55 wt% and P_2O_5 at 37 wt% as calcium phosphate; MgO at 41 wt% as olivine; and TiO_2 at 70 wt% as ilmenite–rutile. We also compared oxide abundances of YDB spherules with those of SLOs, but found no significant compositional differences, consistent with formation from similar source minerals (SI Appendix, Fig. S204). Similarly, we investigated whether SEM/EDS surface analyses were different from those of cross-sections, but found no significant differences (SI Appendix, Fig. S20B), indicating that most individual YDB objects are relatively homogeneous.

Our SEM/EDS analyses allow YDB spherules and SLOs to be grouped into two general compositional categories: those enriched in Fe and those enriched in Al–Si, with significant mixing between categories (SI Appendix, Figs. S19A and S21A), e.g., occasionally, Al–Si–rich cores were surrounded by thin high-Fe rims. A flowchart illustrating identification parameters for the two types is shown in SI Appendix, Fig. S22. The Fe-rich group is dominated by crystalline minerals requiring high temperatures, including magnetite (Fe_3O_4 , melting point $> 1,550$ $^\circ\text{C}$), hematite (Fe_2O_3 , $> 1,550$ $^\circ\text{C}$), titanomagnetite (Fe_2TiO_4 , $> 1,400$ $^\circ\text{C}$), schreibersite [$(\text{Fe,Ni})_3\text{P}$, $> 1,400$ $^\circ\text{C}$], hercynite (FeAl_2O_4 , $> 1,700$ $^\circ\text{C}$), rutile (TiO_2 , $> 1,840$ $^\circ\text{C}$), native Fe ($> 2,000$ $^\circ\text{C}$), and suessite (Fe_3Si , $> 2,300$ $^\circ\text{C}$) (8, 35, 43). The Al–Si–rich group is typically represented by minerals such as high-temperature wollastonite (CaSiO_3 , melting point $> 1,500$ $^\circ\text{C}$), corundum (crystalline Al_2O_3 , $> 1,800$ $^\circ\text{C}$), mullite ($3\text{Al}_2\text{O}_3 \cdot 2\text{SiO}_2$ and $2\text{Al}_2\text{O}_3 \cdot \text{SiO}_2$, $> 1,800$ $^\circ\text{C}$), sillimanite (Al_2SiO_5 , $> 1,800$ $^\circ\text{C}$), and lechatelierite (SiO_2 glass, $> 2,200$ $^\circ\text{C}$ for low-viscosity flow) (8, 35, 43). Because YDB objects contain multiple oxides that are not in equilibrium, the liquidus temperatures may be lower than indicated. Even so, the complete

assemblage of minerals in YDB objects is inconsistent with non-impact terrestrial origins, where maximum temperatures are too low (8). The results are consistent with formation by high-temperature, hypervelocity airbursts/impacts.

Potential Biases Favoring Fe-Rich Spherules. In previous spherule work, it was observed that the abundance ratio of Fe-rich spherules to Si-rich ones may suffer from various biases (42). The first bias is magnetic separation bias, which is known to decrease the observed number of nonmagnetic, Si-rich ocean spherules, but is estimated to decrease the totals by only $\sim 10\%$ (42), a negligible bias. YDB spherules ≥ 200 μm were usually collected by sieving, and therefore unaffected by magnetic bias. However, spherules < 200 μm were typically collected using magnets, and therefore the number of Fe-rich spherules was almost certainly enhanced. The second bias is selection bias. When searching for YDB spherules, it is easier to detect small, dark Fe-rich spherules than lighter Si-rich ones (7, 13), creating a potential cognitive bias. However, experiments designed to detect Si-rich spherules suggest that this bias is negligible, estimated at $< 10\%$. The third bias is fractionation bias, due to the melting and cooling of impact material. When boiling impact rock is transported rapidly through the atmosphere, FeO tends to migrate to the rim (41) and may ablate as small spherules, potentially increasing the relative percentage of Fe-rich spherules. Finally, there is preservation bias. Fe-rich spherules are less susceptible to chemical or mechanical alteration than Si-rich spherules; this is observed for Si-rich stony meteorites that decompose with a half-life of 10–15 ky in dry areas of continents (44), and in as little as 2 ky in wetter environments, whereas Ni-Fe meteorites decompose far more slowly. After 13 ky on land, the majority of Si-rich YDB objects may have suffered such decomposition, artificially increasing the ratio of Fe to Si spherules.

To investigate potential preservation biases, we plotted FeO concentrations against spherule diameters. For sites with active depositional paleoenvironments (e.g., rivers, streams, and dunes), all YDB objects averaged 86 wt% FeO, whereas sites with less active paleoenvironments had an average of 25 wt% FeO, $\sim 3.4\times$ less (SI Appendix, Fig. S21 B and C and Table S6). For YDB objects < 50 μm , FeO was 77 wt%, whereas for YDB objects ≥ 200 μm in all paleoenvironments, the average FeO abundance was 15 wt%, $\sim 5\times$ less (SI Appendix, Table S6). This disparity reveals that Al–Si–rich spherules are significantly underrepresented both in the < 50 - μm group and at sites with active paleoenvironments, most likely due to the preferential destruction over time of smaller Al–Si–rich spherules, producing a bias in favor of Fe-rich spherules. We conclude that compositions of spherules and SLOs of ≥ 200 μm are more representative of parent YDB impact materials, and we use those for comparison below with most reference materials.

Potential Origin of YDB Objects by Cosmic Flux. To explore the hypothetical origin of YDB spherules by meteoritic ablation or cosmic influx (10, 11, 34), we compiled data for known cosmic material. First, we compared elemental abundances of 605 previously reported Al–Si–rich cosmic spherules (all < 67 wt% FeO)

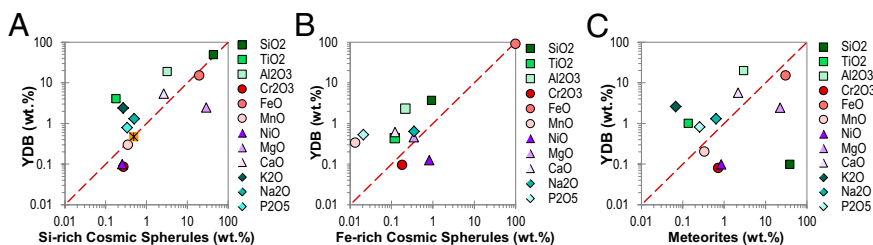


Fig. 4. Comparison of oxide weight percentages; red line marks equivalent values. YDB spherule subsets are in same range for comparability. (A) Comparison with Si-rich cosmic spherules (< 67 wt% FeO). (B) Comparison with Fe-rich cosmic spherules (> 63 wt%). (C) YDB objects ≥ 200 μm compared with meteorites and micrometeorites. Some values differ by $> 10\times$. Data in SI Appendix, Tables S6 and S7.

with Al-Si-rich YDB objects (a subset at <67 wt% FeO, for comparability; Fig. 4A; *SI Appendix, Table S6*). Most cosmic Si-rich spherules derive from the most common type of cosmic object, stony meteorites, which are enriched in MgO, so that ~98% of those spherules have >10 wt% MgO (average: 29%; range: 1–55%; *SI Appendix, Fig. S23A*) (45, 46). Similarly, ~90% of grains captured from the near-Earth stony asteroid Itokawa had >10 wt% MgO (47), and cometary material captured from Comet 81P/Wild 2 included extraterrestrial grains that averaged 35 wt% MgO (range: 21–55%) (48). By comparison, only ~0.2% of 626 measurements on YDB spherules had >10% MgO, indicating almost none originated from stony meteorites.

We also compared elemental abundances of 90 Fe-rich cosmic spherules having >63 wt% FeO with YDB objects (subset >63 wt% FeO), but found them to be dissimilar (Fig. 4B; *SI Appendix, Table S6*). For example, Ni is common in Ni-Fe meteorites with an average concentration of 10 wt% (range: 5–25 wt%) (49), whereas Ni is depleted 100× in YDB spherules with an average concentration of 0.1 wt% (range: 0–2 wt%). None of the YDB objects (184 EDS cross-sectioned; 441 EDS whole) have concentrations of Ni of >1 wt%, demonstrating a poor match for Ni-Fe meteorites. We also compared elemental abundances of YDB objects ≥ 200 μm with 262 different meteorites and micrometeorites, finding a poor match (Fig. 4C; *SI Appendix, Table S6*). Furthermore, most meteorites except, for example, those from the Moon and Mars, have low percentages of TiO₂, averaging >0.14 wt%. YDB spherules with diameter <50 μm averaged 5.0 wt% TiO₂, or 35× higher, and 26 of those had average TiO₂ of 41 wt% (range: 12–70 wt%), including those exhibited in Fig. 3 B, R, and L. Together, the geochemical comparisons indicate that the vast majority of YDB objects are unlikely to have formed from material found in known stony asteroids, Ni-Fe meteorites, or comets, but that does not preclude formation of spherules from target rocks during impacts by such objects.

We compared abundances of YDB spherules with the influx rate of cosmic spherules observed in the Antarctic ice sheet. The 1991 European Meteorite Collection Program Antarctic Expedition discovered an average of only one cosmic spherule in 67 kg (0.015 spherules per liter) (50) of continuously deposited preindustrial ice. In contrast, the average value for the YDB layer is 955 spherules per kilogram, or 67,000× higher. Similarly, Badyukov et al. (51) calculated the terrestrial flux rate of cosmic spherules at one spherule per square centimeter of Earth's surface per 1–2 million years. For the YDB layer with an average density of 6.3 spherules per square centimeter, this flux rate would require >6 million years to produce the observed accumulation of YDB spherules. As one proposed explanation, some researchers (10, 11, 34) have countered that the apparent concentrations of YDB spherules may result from formation of lag deposits that accumulated over thousands to millions of years on a geologically stable surface. However, based on age-depth models for YDB sites that show no significant hiatuses, and based on the paucity of spherules outside of the YDB, that hypothesis is not supported by the age-depth models in *SI Appendix, Figs. 2–15*. Cosmic spherules appear to comprise an extremely small percentage of YDB spherules.

Potential Anthropogenic Origin of YDB Spherules. To evaluate the proposed anthropogenic origin of YDB materials (34), we studied one of the most common industrial contaminants, fly ash grains ($n = 143$ EDS) and anthropogenic spherules ($n = 42$ EDS) from 13 countries in North America and Europe. If YDB spherules are anthropogenic, then they are young and would not have experienced degradation of Si-rich spherules in sediment; consequently, we compared the anthropogenic material to all YDB spherules and SLOs. YDB objects contain more Fe (5×), Cr (9×), and Mn (×5) than fly ash and related spherules, and thus are unlikely to be anthropogenic (Fig. 5A). Additionally, most YDB layers were located at depths of 2–15 m, and great care was taken during sample collection to reduce the possibility of anthropogenic contamination. Furthermore, millimeter-sized airborne objects tend to fall out of the atmosphere close to their source (8), and there are no major anthropogenic sources sufficiently close to most of the 18 study sites. Therefore, YDB spherules with diameters of up to 5.5 mm are inconsistent with long-range atmospheric transport of anthropogenic materials. In addition, when temporally diagnostic cultural artifacts and/or megafaunal remains were present at sampling locations, there was no indication of displacement of the YDB layers, indicating that contamination by modern materials is unlikely. We conclude that the majority of YDB spherules were found in situ, and that anthropogenic glass or spherules represent a small percentage of the assemblage, if any.

Potential Volcanic Origin of YDB Spherules. We compiled >10,000 compositional analyses of volcanic glass and spherules from sites in four oceans. Compositions of YDB objects ≥ 200 μm are higher in oxides of Cr (8×) and K (11×) and lower in Mg (3×) and Na (2×) than volcanic material, and thus are geochemically dissimilar (Fig. 5B). YDB compositions are also enriched in K (89×) and P (37×) over mantle material (52). This poor correspondence indicates that YDB objects are not comprised of volcanic or mantle material (Fig. 5C). The YDB layers and contiguous strata at 18 sites also do not contain visible tephra or volcanogenic silica (tridymite) that typically occurs as bipyramidal euhedral crystals. In summary, it is unlikely that a volcanic eruption could have deposited millions of tonnes of volcanic spherules across a 12,000-km-wide region without leaving any other mineralogical, geochemical, or geological evidence.

Potential Origin of YDB Spherules by Lightning. Another hypothesis for spherule formation is that the YDB spherules formed through atmospheric lightning discharges (53). Besides cosmic impact, lightning is the only documented process that can account for lechatelierite inside YDB spherules (54). Such discharges generate intense magnetic fields, and after rapid cooling of lightning-melted spherules, strong magnetic characteristics should remain (53, 55, 56). Even though formation by lightning is unlikely given the wide geographical distribution of YDB spherules and the paucity of lightning melt products (e.g., fulgurites) above, below, or inside the YDB, we measured the magnetic characteristics of YDB spherules from two sites: Gainey, Michigan, and Blackwater Draw, New Mexico. To pre-

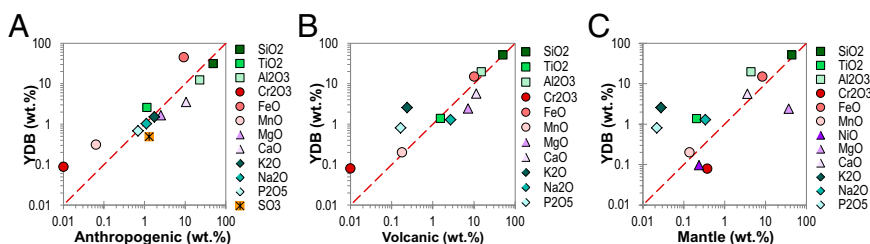


Fig. 5. Comparison of compositions of YDB spherules and SLOs with (A) anthropogenic spherules and fly ash, (B) YDB objects ≥ 200 μm compared with volcanic glass and spherules, and (C) material from Earth's mantle. Red dashed line marks equivalent values. Note that some values differ by more than an order of magnitude. Data shown are in *SI Appendix, Tables S6 and S7*.

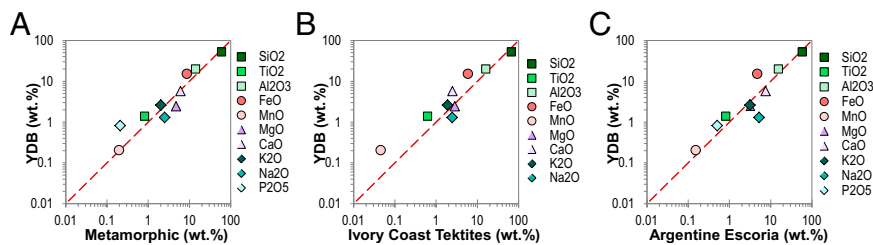


Fig. 6. Comparison of composition of YDB spherules and SLOs at $\geq 200 \mu\text{m}$ with (A) metamorphic rocks; (B) Ivory Coast tektites; and (C) Argentine Escoria. Red dashed line represents equivalent values. Data shown are in *SI Appendix, Tables S6 and S7*.

serve the spherules original magnetic state, nonmagnetic separation techniques were used (heavy liquids), followed by non-magnetic, mechanical separation that was performed using sieves of various sizes (~ 37 , 44 , 74 , and $149 \mu\text{m}$). The separates were cleaned of excess clay using ultrasonication and then analyzed under an optical microscope. When candidate spherules were identified, they were manually placed on glass plates and examined using SEM. Remanent magnetization in the spherules was measured using a magnetic scanner and a superconducting magnetometer. There was no excess magnetization of the spherules while in Earth's ambient geomagnetic field ($50 \mu\text{T}$). However, after being subjected to a powerful laboratory-generated magnetic field (1 T), the YDB spherules displayed substantial remanent magnetization, indicating their ability to become magnetized toward saturation (*SI Appendix, Fig. S24*). These

results are consistent with the hypothesis that when the spherules formed during an extraterrestrial impact, they were subjected only to the ambient geomagnetic field, and exclude the possibility that these spherules formed during lightning discharges.

Evidence for an Impact Origin of YDB Spherules. If an impact occurred at the YD onset, then YDB spherules should be geochemically similar to terrestrial rocks and sediment, and to investigate that, we compared spherule compositions with those of $>100,000$ samples of terrestrial sediments and minerals from across North America, including sedimentary, igneous, and metamorphic rocks from the US Geological Survey National Geochemical Database (59, 60). YDB spherules are compositionally similar to surficial sediments and metamorphic rocks, e.g., mudstone, shale, gneiss, schist, and amphibolite (Fig. 6A; *SI Appendix, Table S6*), which suggests that YDB objects formed by the melting of heterogeneous surficial sediments comprised of weathered metamorphic and other similar rocks. This is consistent with a cosmic impact, in which the impactor contributed an unknown percentage of material.

We also reviewed $>1,000$ analyses of impact-related material, including spherules and tektites—melt-glasses that typically contain lechatelierite—to compare the YDB event with 12 known craters and strewnfields on six continents. Some melt-glasses (Argentine Escoria and Dakhleh glass) are morphologically similar to YDB SLOs (8), whereas other types are not (Australasian tektites and moldavites from Ries Crater). Most tektites are derived from melted surficial sediments and/or metamorphic rocks, typically comprised of silicates, limestone, shale, and/or clay (61, 62). The compositions of YDB objects are different from the KPg and Chesapeake Bay impactites, but similar to Ivory Coast tektites (Fig. 6B), Argentine Escoria (Fig. 6C), Tasman Sea tektites (*SI Appendix, Fig. S23B*), and Tunguska spherules (*SI Appendix, Fig. S23C and Table S6*).

YDB spherules and SLOs also are morphologically and compositionally similar to spherule-rich materials, called trinitite, produced by the melting of surficial sediments by two nuclear aerial detonations (8). One detonation was at the Trinity site near Socorro, New Mexico (36, 37), and the other at Yucca Flat, Nevada (63); both were near-surface airbursts rather than below-ground detonations. Trinity produced highly abundant spherules from a crater that was 80 m wide and 1.4 m deep, providing an analog for a cosmic airburst/impact (8). The thermal pulse and air shock were produced by different mechanisms (a rapidly moving cosmic object vs. a pulse of atomic radiation), but even so, the resulting melted material is indistinguishable.

To investigate the thermochemical history of the spherules, we reviewed the work of Elkins-Tanton et al. (41, §), who analyzed cross-sectioned spherules from five known impact events (Australasian, Ries, Bosumtwi, Chesapeake Bay, and Popigai) and

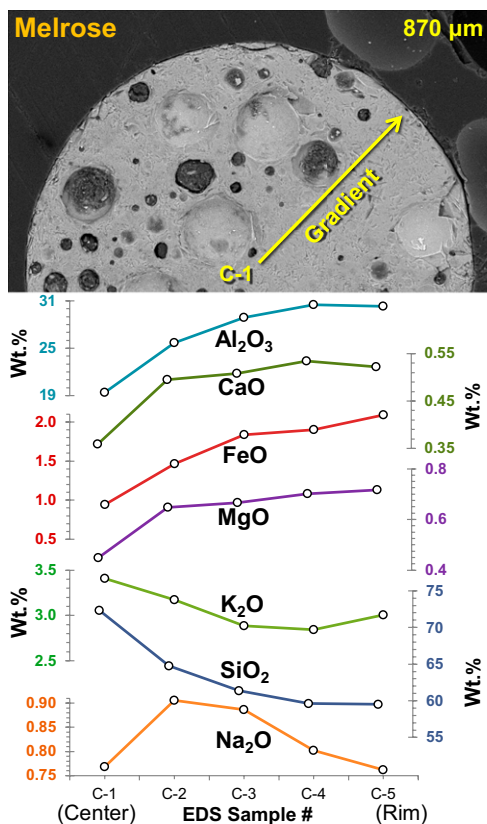


Fig. 7. Melrose spherule with diameter in yellow, showing approximate radial traverse for seven EDS analyses. Refractory oxides (Al, Ca, Fe, and Mg) increase toward rim; less-refractory oxides (Si and K) decrease toward rim. Na weight percentages are mixed, but generally decrease. These variations are consistent with boiling rock at temperatures of $\sim 2,200 \text{ }^\circ\text{C}$ to $3,600 \text{ }^\circ\text{C}$. Data are in *SI Appendix, Table S8*.

[§]Elkins-Tanton LT, Kelly DC, Bico J, Bush JWM, Microtektites as vapor condensates, and a possible new strewn field at 5 Ma. Thirty-Third Annual Lunar and Planetary Science Conference, March 11–15, 2002, Houston, TX, abstr 1622.

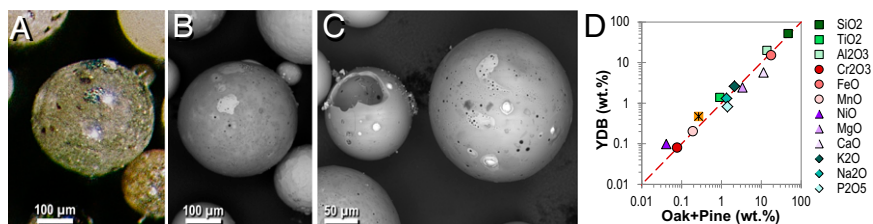


Fig. 8. Al-Si-rich laboratory spherules made at $>1,730$ °C. (A) Micrograph of oak spherules; largest = 350 μm . (B) SEM image of same oak spherule group. (C) SEM image of pine spherules; largest = 220 μm . (D) YDB objects ≥ 200 μm compared with Al-Si-rich oak and pine. Red dashed line represents equivalent values. Data shown are in *SI Appendix, Tables S6 and S7*.

found that each spherule displayed compositional gradients between the rim and center. The authors argued that the gradients resulted from two processes, the first of which, vaporization, occurred when surface tension shaped boiling impact rock into spherules, after which constituent oxides vaporized at varying rates. Refractory oxides, such as MgO (boiling point: 3,600 °C), FeO (3,414 °C), Al₂O₃ (2,980 °C), and CaO (2,850 °C) (43) reached their boiling points later and became enriched toward the rim. Conversely, SiO₂ (2,230 °C) and Na₂O (1,950 °C) usually were depleted toward the rim because of their lower boiling points. The second process, condensation, occurred as various oxides or elements condensed from their vapor state to form spherules. According to Elkins-Tanton et al. (41), condensation had the opposite effect on composition, because higher-temperature oxides condensed from vapor to liquid earliest as plume temperatures fell, producing enrichment at the center of the spherule, and lower-temperature oxides or elements condensed from vapor last, becoming enriched toward the rim. For condensation, the presence of a reverse gradient implies that temperatures of the melted rock possibly were $>3,600$ °C, the boiling point of MgO.

To investigate whether compositional gradients are present in YDB spherules, we acquired data on 4–5 points along a radius from center to rim of cross-sectioned spherules from three sites (Abu Hureyra, Blackville, and Melrose). For 11 of the 13 spherules analyzed (85%), there were discernible gradients of oxide values (Fig. 7; *SI Appendix, Fig. S25 and Table S8*): 7 of 13 displayed generally decreasing trends for SiO₂, indicating boiling; 4 of 13 displayed increasing trends for SiO₂, suggesting condensation; and 2 of 13 displayed no clear gradients. Oxides with abundances of less than a few percent were more variable, presumably due to high analytical uncertainties. Nearly all oxides behaved predictably, but occasionally, one or more oxides displayed an opposite trend to that predicted, for reasons that are unclear. Several spherules displayed a distinct high-Fe shell a few microns thick surrounding an Al-Si interior, presumably due to condensation, ablation, or accretion. The presence of both increasing and decreasing gradients in YDB spherules suggests that there were sufficiently high temperatures and flight times for vaporization and condensation to occur. No plausible process besides a cosmic airburst/impact is capable of boiling or vaporizing airborne rock at $>2,200$ °C long enough to produce millimeter-sized spherules that display compositional gradients.

Possible Spherule Formation by Impact-Related Wildfires. Burleigh and Meeks (35) reported the formation of glassy spherules by combustion of wood charcoal, and speculated that temperatures $>2,000$ °C were required for optimum spherule production. We explored this possible origin for YDB spherules by conducting wood-burning laboratory experiments using an oxygen/propylene burner with a maximum temperature of $\sim 2,900$ °C; temperatures were confirmed using pyrometry. For the wood source, we used dried twigs of oak (*Quercus turbinella*) and pine (*Pinus ponderosa*) with a diameter of 0.5–1.0 cm.

At temperatures of $\sim 1,600$ °C, the flame transformed the wood into charcoal and then rapidly to whitish-gray ash. At $\sim 1,730$ °C, the melting point of SiO₂, the ash began to melt and transform by surface tension into spherules that were ejected from the twig by flame pressure (Fig. 8A and B). Spherule production increased up to 2,600 °C, the maximum temperature measured. Within a few minutes, a small twig (6 \times 0.5 cm) produced >600 spherules, ranging in diameter from 30 to 700 μm , with the majority at the lower end of that range (50–80 μm). Of the original weight of oak and pine, $\sim 97\%$ was transformed into water vapor and other gases, $\sim 1\%$ remained as ash, and $\sim 2\%$ by weight of spherules were formed from biogenic silica and other trace mineral oxides (e.g., Al, Si, and Ca). Most of the melted objects formed as spherules, although a small percentage ($<5\%$) formed as aerodynamically shaped teardrops and ovoids; often, multiple spherules fused together. Colors included black, brown, red, blue, green, gray, tan, and white, with clarity ranging from opaque to transparent. Nearly all spherules are highly vesicular, and some are hollow with a thin glass shell (Fig. 8C); some display flow marks or schlieren consistent with high temperatures and low viscosity, as seen in YDB spherules. Average compositions of oak and pine closely match compositions of Al-Si-rich YDB objects (Fig. 8D). Although we observed inclusions of up to 75 wt% FeO, we found no complete high-Fe spherules with Fe quench crystals. These results show that the incineration of biomass at $\sim 1,730$ – $2,600$ °C can produce glassy spherules, and we conclude that a significant percentage of YDB Al-Si-rich spherules could have formed by the impact-related incineration of biomass, but not the high-Fe spherules. The requisite temperature of 1,730 °C is above the maximum temperature ever recorded in a wildfire (8).

Geographical Distribution of Spherules. There are three major impact strewnfields, the largest of which is the 780,000-y-old Australasian tektite field, spanning 50 million square kilometers (Fig. 1; Table 1) (25, 26). Another is the 35-million-y-old North American tektite field, covering 42 million square kilometers and associated with the 85-km-wide Chesapeake Bay crater (25, 26). The last strewnfield is the 970,000-y-old Ivory Coast field, covering 4 million square kilometers and associated with the 10.5-km-wide Bosumtwi crater in Ghana, Africa (Table 1) (25, 26). Although the maximum extent of the YDB field has not yet been established, its known extent is ~ 50 million square kilometers, making it 10 \times larger than the smallest field in Table 1 and equal

Table 1. Comparison of tonnage in the YDB strewnfield with known impact strewnfields

Field name	Age	$\sim\%$ of Earth	Size, km ²	Metric tons	Source
Eocene	~ 35 Ma	8	4.2×10^7	100×10^7	19
Australasian	~ 780 ka	10	5.0×10^7	10×10^7	18
Ivory Coast	~ 970 ka	1	0.4×10^7	2×10^7	18
YDB field	~ 12.9 ka	10	5.0×10^7	1×10^7	This work

in size to the largest one, the Australasian field (Fig. 1). Using standard calculations for determining the mass of spherules deposited in an impact strewnfield (25, 26), and assuming that currently observed average values are representative of the entire field, we estimate the mass of the YDB field to equal ~10 million tonnes; this is approximately half the tonnage of the Ivory Coast field associated with the Bosumtwi Crater (10.5 km wide), thus implying a major impact event (Table 1; computational variables in *SI Appendix, Table S9*).

Preliminary Impact Model. At present, there are insufficient data to characterize the YDB impactor and impact event, and more research is required to determine the type and size of impactor, maximum extent of the strewnfield, and abundances of minor elements. However, existing data suggest the following scenario, as also discussed by Israde et al. (7). The impactor was most likely an asteroid or comet greater than several hundred meters in diameter with maximum size unknown, but probably less than several kilometers in diameter. The impactor most likely broke apart in solar orbit before encountering Earth, as do most comets (64), including Comet Shoemaker–Levy 9, which impacted Jupiter as multiple fragments, the largest of which was ~1 km in diameter. When fragments of the YDB impactor entered Earth's atmosphere, they fragmented even further, yielding multiple atmospheric airbursts that each produced shock fronts. This multi-impact scenario is supported by two lines of evidence: first, the concentrations of multimillimeter-sized YDB melt-glass and spherules in Syria, Pennsylvania, South Carolina (8, 17), Arizona (15), and Venezuela (18–21) are separated by up to 12,000 km. Such multimillimeter-sized, aerodynamically shaped objects are probably too large to have traveled 12,000 km during a single airburst/impact (8). Second, the compositions of YDB objects differ substantially between regions, as indicated in *SI Appendix, Fig. S26*, showing that YDB objects from the relatively close Blackville and Melrose sites are compositionally similar to each other, but dissimilar to those of Abu Hureyra, arguing that multiple airbursts/impacts interacted with different types of regional target rocks.

Beneath the flight path of the impactor fragments, thermal radiation from the air shocks was intense enough to melt Fe-rich and Si-rich surficial sediments, transforming them into lechatelierite-rich melt-glass and spherules at >2,200 °C. Multiple airbursts/impacts over a wide area can account for the heterogeneity of the melt materials. In addition, high temperatures may have produced spherules and melt-glass by incinerating vegetation within the fireballs and shock fronts. High-velocity winds and attenuated air shocks lofted the melted material into the upper atmosphere, where high-altitude winds transported them over a wide area. As previously suggested (7), nanodiamonds potentially formed from vaporized carbon within localized, transiently anoxic regions of the shock front. This impact model is speculative because the exact nature of airbursts is poorly constrained. For example, the complexity of airburst phenomena is only hinted at by the recent hydrocode modeling of Boslough and Crawford (65), who concluded that more realistic airburst simulations are needed to understand the phenomenon.

Methods

To determine replicability of the protocol for magnetic grain and spherule extractions, various samples were processed by nine coauthors (J.P.K., D.J.K., D.F., I.-I.A., J.B.K., Z.R., D.R.K., G.K., and A.W.), using previously published protocol (1, 7, 13). After size-sorting with multiple American Society for Testing and Materials screens, we used a 150–300× reflected light microscope to manually count, photograph, and extract selected spherules. Next, cross-sectioned and whole spherules were examined by 10 coauthors (J.H.W., J.C.V., T.E.B., J.P.K., D.J.K., I.-I.A., J.L.B., R.E.H., G.K., and A.W.), using SEM and EDS to distinguish between impact-related spherules and other types. To ensure acquisition of correct bulk compositions of spherules, EDS analyses were acquired multiple times and/or at large beam spot sizes of ~30 μm. A flow-chart illustrating identification parameters is in *SI Appendix, Fig. S22*. Standard techniques were followed for all analytical methods (*SI Appendix, SI Methods*).

Conclusions

The analyses of 771 YDB objects presented in this paper strongly support a major cosmic impact at 12.8 ka. This conclusion is substantiated by the following:

Spherules and SLOs are (i) widespread at 18 sites on four continents; (ii) display large abundance peaks only at the YD onset at ~12.8 ka; (iii) are rarely found above or below the YDB, indicating a single rare event; and (iv) amount to an estimated 10 million tonnes of materials distributed across ~50 million square kilometers of several continents, thus precluding a small localized impact event.

Spherule formation by volcanism, anthropogenesis, authigenesis, and meteoritic ablation can be rejected on geochemical, morphological, and/or thermochemical grounds, including the presence of lechatelierite (>2,200 °C).

Spherule formation by lightning can be eliminated due to magnetic properties of spherules and the paucity of lightning melt-products (e.g., fulgurites) above or below the YDB.

Morphologies and compositions of YDB spherules are consistent with an impact event because they (i) are compositionally and morphologically similar to previously studied impact materials; (ii) closely resemble terrestrial rock compositions (e.g., clay, mud, and metamorphic rocks); (iii) often display high-temperature surface texturing; (iv) exhibit schlieren and SiO₂ inclusions (lechatelierite at >2,200 °C); (v) are often fused to other spherules by collisions at high-temperatures; and (vi) occasionally display high-velocity impact cratering.

High-temperature incineration of biomass (>1,730 °C) produced laboratory spherules that are similar to YDB spherules, providing a complementary explanation that some unknown percentage of YDB spherules may have formed that way.

Abundances of spherules covary with other YDB impact proxies, including nanodiamonds, high-temperature melt-glass, carbon spherules, aciniform carbon, fullerenes, charcoal, glass-like carbon, and iridium.

The geographical extent of the YD impact is limited by the range of sites available for study to date and is presumably much larger, because we have found consistent, supporting evidence over an increasingly wide area. The nature of the impactor remains unclear, although we suggest that the most likely hypothesis is that of multiple airbursts/impacts by a large comet or asteroid that fragmented in solar orbit, as is common for nearly all comets. The YD impact at 12.8 ka is coincidental with major environmental events, including abrupt cooling at the YD onset, major extinction of some end-Pleistocene megafauna, disappearance of Clovis cultural traditions, widespread biomass burning, and often, the deposition of dark, carbon-rich sediments (black mat). It is reasonable to hypothesize a relationship between these events and the YDB impact, although much work remains to understand the causal mechanisms.

ACKNOWLEDGMENTS. We are grateful for receiving crucial samples, data, and/or assistance from William Topping, Vance Haynes, Joanne Dickinson, Don Simons, Scott Harris, Malcolm LeCompte, Mark Demitroff, Yvonne Malinowski, Paula Zitzelberger, and Lawrence Edge. Bulk sample collection and/or preparation for various sites were conducted by Brendan Culleton, Carley Smith, and Karen Thompson. Dustin Thompson produced an age-depth plot for the Big Eddy site. Ferdi Geerts, Ab Goutbeek, and Henri Jutten provided field assistance in the Netherlands and Belgium. The assistance and support of Keith Hendricks of Indian Trail Caverns (Sheriden Cave), Brian Redmond, and the Cleveland Museum of Natural History are greatly appreciated, as are the suggestions of four anonymous reviewers. Support for this study was provided by the Court Family Foundation, Charles Phelps Taft Foundation, and University of Cincinnati Research Council (K.B.T.); US Department of Energy Contract DE-AC02-05CH11231 and US National Science Foundation Grant 9986999 (to R.B.F.); US National Science Foundation Grants ATM-0713769 and OCE-0825322, Marine Geology and Geophysics (to J.P.K.); and Ministry of Education Youth and Sports Grant LK21303 (to G.K.).

1. Firestone RB, et al. (2007) Evidence for an extraterrestrial impact 12,900 years ago that contributed to the megafaunal extinctions and the Younger Dryas cooling. *Proc Natl Acad Sci USA* 104(41):16016–16021.
2. Kennett DJ, et al. (2008) Wildfire and abrupt ecosystem disruption on California's Northern Channel Islands at the Allerød–Younger Dryas boundary (13.0–12.9 ka). *Quat Sci Rev* 27:2530–2545.
3. Kennett DJ, et al. (2009) Shock-synthesized hexagonal diamonds in Younger Dryas boundary sediments. *Proc Natl Acad Sci USA* 106(31):12623–12628.
4. Kennett DJ, et al. (2009) Nanodiamonds in the Younger Dryas boundary sediment layer. *Science* 323(5910):94.
5. Kurbatov AV, et al. (2011) Discovery of a nanodiamond-rich layer in the Greenland ice sheet. *J Glaciol* 56:749–759.
6. Anderson DG, et al. (2011) Multiple lines of evidence for possible Human population decline/settlement reorganization during the early Younger Dryas. *Quat Int* 242: 570–593.
7. Israde-Alcántara I, et al. (2012) Evidence from central Mexico supporting the Younger Dryas extraterrestrial impact hypothesis. *Proc Natl Acad Sci USA* 109(13):E738–E747.
8. Bunch TE, et al. (2012) Very high-temperature impact melt products as evidence for cosmic airbursts and impacts 12,900 years ago. *Proc Natl Acad Sci USA* 109(28): E1903–E1912.
9. Jones TL, Kennett DK (2012) A land impacted? The Younger Dryas boundary event in California. *Contemporary Issues in California Archaeology*, eds Jones TL, Pery JE (Left Coast, Walnut Creek, CA), pp 37–48.
10. Surovell TA, et al. (2009) An independent evaluation of the Younger Dryas extraterrestrial impact hypothesis. *Proc Natl Acad Sci USA* 106(43):18155–18158.
11. Pinter N, et al. (2011) The Younger Dryas impact hypothesis: A requiem. *Earth Sci Rev* 106:247–264.
12. Boslough MBE, et al. (2012) Arguments and evidence against a Younger Dryas Impact Event. *Geophys Monogr Ser* 198:13–26.
13. LeCompte MA, et al. (2012) Independent evaluation of conflicting microsphere levels from different investigations of the Younger Dryas impact hypothesis. *Proc Natl Acad Sci USA* 109(44):E2960–E2969, 10.1073/pnas.1208603109.
14. Pigati JS, et al. (2012) Accumulation of impact markers in desert wetlands and implications for the Younger Dryas impact hypothesis. *Proc Natl Acad Sci USA* 109(19): 7208–7212.
15. Fayek M, Anovitz LM, Allard LF, Hull S (2012) Framboidal iron oxide: chondrite-like material from the black mat, Murray Springs, Arizona. *Earth Planet Sci Lett* 319–320: 251–258.
16. Haynes CV, Jr., et al. (2010) The Murray Springs Clovis site, Pleistocene extinction, and the question of extraterrestrial impact. *Proc Natl Acad Sci USA* 107(9):4010–4015.
17. Wu Y (2011) Origin and provenance of magnetic spherules at the Younger Dryas boundary. PhD thesis (Dartmouth College, Hanover, NH).
18. Mahaney WC, Kirsinsley D (2012) Extreme heating events and effects in the natural environment: Implications for environmental geomorphology. *Geomorphology* 139–140:348–359.
19. Mahaney WC, et al. (2010) Evidence from the northwestern Venezuelan Andes for extraterrestrial impact: The black mat enigma. *Geomorphology* 116(1–2):48–57.
20. Mahaney WC, et al. (2011) Fired glacioluvial sediment in the northwestern Andes: Biotic aspects of the Black Mat. *Sediment Geol* 237(1–2):73–83.
21. Mahaney WC, et al. (2011) Notes on the black mat sediment, Mucunuque Catchment, northern Mérida Andes, Venezuela. *J Adv Microscop Res* 6(3):177–185.
22. Wright FW, Hodge PW (1965) Studies of particles for extraterrestrial origin, Part 4. Microscopic spherules from recent volcanic eruptions. *J Geophys Res* 70(16): 3889–3898.
23. Scott AC, et al. (2010) Fungus, not comet or catastrophe, accounts for carbonaceous spherules in the Younger Dryas “impact layer”. *Geophys Res Lett* 37(14):L14302.
24. Daulton TL, Pinter N, Scott AC (2010) No evidence of nanodiamonds in Younger-Dryas sediments to support an impact event. *Proc Natl Acad Sci USA* 107(37):16043–16047.
25. Glass BP, Swincki MB, Zwart PA (1979) Australasian, Ivory Coast and North American tektite strewnfields: Size, mass and correlation with geomagnetic reversals and other earth events. *Proceedings of the 10th Annual Lunar Planet Science Conference* (Pergamon, New York), pp 2535–2545.
26. Glass BP, Burns CA, Crosbie JR, DuBois DL (1985) Late Eocene North American microtektites and clinopyroxene-bearing spherules. *J Geophys Res* 90(S01):D175–D196.
27. Glass BP, Huber H, Koeberl C (2004) Geochemistry of Cenozoic microtektites and clinopyroxene-bearing spherules. *Geochim Cosmochim Acta* 69:3971–4006.
28. Mathur SC, Gaur SD, Loyal RS, Tripathi A, Sisodia MS (2005) Spherules from the Late Cretaceous phosphorite of the Fatehgarh Formation, Barmer Basin, India. *Gondwana Res* 8:579–584.
29. Korchagin OA (2010) Metallic microspheres and microparticles in lower Cenomanian sediments of the Crimea: Evidence for the cosmic dust event. *Dokl Earth Sci* 431(Pt 2): 441–444.
30. Smit J (1990) Meteorite impact, extinctions and the Cretaceous-Tertiary boundary. *Geol Mijnb* 69:187–204.
31. Mukhopadhyay R, Iyer SD, Ghosh AK (2002) The Indian Ocean nodule field: Petrotectonic evolution and ferromanganese deposits. *Earth Sci Rev* 60:67–130.
32. Thy P (1995) Implications of prehistoric glassy biomass slag from east-central Botswana. *J Archaeol Sci* 22:629–637.
33. Hein JR, Griggs GB (1972) Distribution and scanning electron microscope (SEM) observations of authigenic pyrite from a Pacific deep-sea core. *Deep Sea Res* 19(2): 133–138.
34. Del Monte M, Sabbioni C (1984) Morphology and mineralogy of fly ash from a coal-fueled power plant. *Arch Met Geoph Biocl B* 35(1–2):93–104.
35. Burchfield R, Meeks N (1986) Glassy microspherules from bomb combustion of charcoal. *Radiocarbon* 28(1):165–166.
36. Eby N, Hermes R, Charnley N, Smoliga JA (2010) Trinitite—the atomic rock. *Geol Today* 26:181–186.
37. Hermes RE, Strickfaden WB (2005) A new look at trinitite. *Nucl Weap J* 2:2–7.
38. Wasson JT (2003) Large aerial bursts: An important class of terrestrial accretionary events. *Astrobiology* 3(1):163–179.
39. Waters MR, Stafford TW, Jr. (2007) Redefining the age of Clovis: Implications for the peopling of the Americas. *Science* 315(5815):1122–1126.
40. Haynes CV, Jr. (2008) Younger Dryas “black mats” and the Rancholabrean termination in North America. *Proc Natl Acad Sci USA* 105(18):6520–6525.
41. Elkins-Tanton LT, Aoussilous P, Bico J, Quere D, Bush JWM (2003) A laboratory model of splash-form tektites. *Meteorit Planet Sci* 38(9):1331–1340.
42. Brownlee DE, Bates B, Schramm L (1997) The elemental composition of stony cosmic spherules. *Meteorit Planet Sci* 32:157–175.
43. Kracek FC (1963) Melting and transformation temperatures of mineral and allied substances. *Geological Survey Bulletin 1144-D* (US Government Printing Office, Washington, DC).
44. Jull AJT, Donahue DJ, Cielaszyk E, Wlotzka F (1993) Carbon-14 terrestrial ages and weathering of 27 meteorites from the southern high plains and adjacent areas (USA). *Meteoritics* 28(2):188–195.
45. Taylor S, Brownlee DE (1991) Cosmic spherules in the geologic record. *Meteoritics* 26: 203–211.
46. Taylor S, Lever JH, Harvey RP (2000) Numbers, types, and compositions of an unbiased collection of cosmic spherules. *Meteorit Planet Sci* 35:651–666.
47. Nakamura E, et al. (2012) Space environment of an asteroid preserved on micrograins returned by the Hayabusa spacecraft. *Proc Natl Acad Sci USA* 109(11):E624–E629.
48. Flynn GJ, et al. (2006) Elemental compositions of comet 81P/Wild 2 samples collected by Stardust. *Science* 314(5806):1731–1735.
49. Daode W, Yongheng C (1996) The chemical compositions of Antarctic iron meteorites and their classification. *Advances in Polar Science* 7:41–49.
50. Maurette M, Pourchete M, Perreau M (1992) The 1991 EUROMET microtektite collection at Cap-Prudhomme, Antarctica. *Meteoritics* 27:473–475.
51. Badyukov DD, Ivanov AV, Raitala J, Khisina NR (2011) Spherules from the Tunguska event site: Could they originate from the Tunguska Cosmic Body? *Geochem Int* 49: 641–653.
52. McDonough WF (1991) Chemical and isotopic systematics of continental lithospheric mantle. *Kimberlites, Related Rocks and Mantle Xenoliths*, eds Meyer HOA, Leonardos OH (Companhia de Pesquisa de Recursos Minerais, Rio de Janeiro), Vol 1, pp 478–485.
53. Kletetschka G (2001) Electric discharge in carbonaceous meteorites? *First Steps in the Origin of Life in the Universe*, eds Chela-Flores J, et al. (Springer, Dordrecht), pp 157–159.
54. French BM (1998) *Traces of Catastrophe: A Handbook of Shock-Metamorphic Effects in Terrestrial Meteorite Impact Structures*. LPI Contribution No. 954 (Lunar and Planetary Inst, Houston), pp 102–103.
55. Kletetschka G, Kohout T, Wasilewski PJ (2003) Magnetic remanence in the Murchison meteorite. *Meteorit Planet Sci* 38(3):399–405.
56. Wasilewski P, Kletetschka G (1999) Lodestone: Nature's only permanent magnet—what it is and how it gets charged. *Geophys Res Lett* 26(15):2275–2278.
57. Kletetschka G et al. (2006) TRM in low magnetic fields: a minimum field that can be recorded by large multidomain grains. *Phys Earth Planet In* 154(3–4):290–298.
58. Wasilewski P, Acuna MH, Kletetschka G (2002) 433 Eros: Problems with the meteorite magnetism record in attempting an asteroid match. *Meteorit Planet Sci* 37(7):937–950.
59. US Geological Survey (2001) *Geochemistry of Soils in the US from the PLUTO Database* (USGS, Reston, VA).
60. US Geological Survey (2008) *Geochemistry of Rock Samples from the National Geochemical Database* (US Geological Survey, Reston, VA), <http://mrdata.usgs.gov/ngdb/rock/>.
61. Koeberl C (1986) Geochemistry of tektites and impact glasses. *Annu Rev Earth Planet Sci* 14:323–350.
62. Claeys P, Casier J-G (1994) Microtektite-like impact glass associated with the Frasnian-Famennian boundary mass extinction. *Earth Planet Sci Lett* 122:303–315.
63. Glass BP, Senffle FE, Muenow DW, Aggrey KE, Thorpe AN (1987) Atomic bomb glass beads: Tektite and microtektite analogs. *Proceedings of the Second International Conference on Natural Glasses*, ed Konta J (Charles Univ, Prague), pp 361–369.
64. Napier WM (2010) Palaeolithic extinctions and the Taurid Complex. *Mon Not R Astron Soc* 405:1901–1906.
65. Boslough MBE, Crawford DA (2008) Low altitude airbursts and the impact threat. *Int J Impact Eng* 35(12):1441–1448.